Analysis of parameter combinations for optimal soliton microcomb generation efficiency in a simple single-cavity scheme

Nikita M. Kondratiev [1,*] Valery E. Lobanov [2] Nikita Yu. Dmitriev,[2] Steevy J. Cordette [1] and Igor A. Bilenko[2,3]

[1]*Directed Energy Research Centre, Technology Innovation Institute, Abu Dhabi, United Arab Emirates*
[2]*Russian Quantum Center, 143026 Skolkovo, Russia*
[3]*Faculty of Physics, Lomonosov Moscow State University, 119991 Moscow, Russia*

Dissipative Kerr solitons generated in high-Q optical microresonators provide unique opportunities for different up-to-date applications. Increasing the generation efficiency of such signals is a problem of paramount importance. We perform a comprehensive analytical and numerical analysis using a simple single-cavity scheme. It is revealed that in order to obtain high pump-to-comb conversion efficiency such parameters as coupling rate, pump amplitude, detuning, and microresonator second-order dispersion should not be considered individually, only in the aggregate. The dependence of the optimal coupling rate on the pump power is shown, in addition to the trade-off relations balancing the efficiency versus the number of comb lines. Combining analytical predictions and numerical simulations, we find optimal conditions for the maximal pump-to-comb conversion efficiency (up to 100%) in the cases of free-running and self-injection-locked pump lasers. The discrepancy between numerical and analytical solutions and methods to increase the total comb power are also discussed.

I. INTRODUCTION

Microresonator-based frequency combs or microcombs [1–6] are promising tools for numerous applications, including time-frequency metrology, optical frequency synthesis, spectroscopy, communication, and quantum technologies [7–13]. Coherent frequency combs, or dissipative solitons in temporal representation, are of particular interest. Unfortunately, the most accessible coherent frequency combs in the form of bright dissipative Kerr solitons [12] are realizable in the anomalous group-velocity-dispersion (GVD) regime and suffer from a low pump-to-comb conversion efficiency which was long commonly known to be no more than 10% [12,14]. To overcome this limitation, special feedback schemes [15,16], normal dispersion usage [17–20], and pulsed pumping [21] have been suggested.

However, recent studies demonstrated that it is possible to reach values up to 40% [22,23] even without any special schemes, showing that this problem has not been fully investigated, and no fundamental limit of the conversion efficiency has been clearly defined. Although previous studies concerned the dependence of the pump conversion efficiency on the microresonator free spectral range (FSR) [23] or the input power and the coupling rate [24,25], those dependences were usually treated independently, and only general trends were shown. In reality, both FSR and coupling rate influence the threshold power: the former through the mode volume and the latter through the loaded quality factor. Furthermore, restrictions should be applied to the coupling rate and the pump power in order to keep the system above the comb generation threshold.

This suggests a nontrivial optimization problem that has never been addressed. We also note that all previous works relied on the simple hyperbolic-secant-squared form of the soliton [26], which is known to be a good approximation only for rather large values of pump detuning and amplitude.

In this paper we use a simple analytical approach to identify the regions of high soliton microcomb generation efficiency considering the combination of significant parameters of the system "laser microresonator" and then verify and amend the obtained results numerically. We demonstrate how the pump power, pump frequency, laser-to-microresonator coupling rate, and second-order dispersion of the microresonator interplay to allow up to a 100% high conversion without any additional schemes, but at the cost of the number of comb lines. Effective methods to increase the total comb power are also discussed. An analysis is performed for the cases of the free-running [26] and self-injection-locked [27–29] pump lasers. We also show that moderate backscattering that is necessary for self-injection locking does not suppress high conversion.

II. CONVERSION EFFICIENCY

We begin by defining the conversion-efficiency figure of merit. Two main definitions of comb generation efficiency can be found in the literature: the pump-to-total-comb (pump-to-soliton) generation efficiency η_{p2s} [23,24,30] and pump-to-comb (pump-to-sideband) generation efficiency η_{p2c} [16,17]. The first variant is more straightforward from a theoretical point of view, as in an analytical approximation the field can be naturally decomposed into a soliton part and a background part. In this temporal representation, the background is just a constant field (stationary single-mode

---
*nikita.kondratyev@tii.ae

solution) a_{st}, whereas the soliton part is a field with a train of hyperbolic-secant pulses, each having the spectral components

$$a_\mu = \sqrt{\frac{d_2}{2}} \operatorname{sech}\left(\frac{\pi \mu}{2}\sqrt{\frac{d_2}{\zeta}}\right) e^{i\psi^{\mathrm{sol}}}, \qquad (1)$$

$$\psi^{\mathrm{sol}} = \arctan \frac{\sqrt{2\pi^2 f^2 \zeta - 16\zeta^2}}{4\zeta}, \qquad (2)$$

where $d_2 = D_2/\kappa$ is the normalized GVD coefficient (assuming the microresonator eigenfrequencies $\omega_\mu = \omega_0 + D_1\mu + D_2\mu^2/2$, where ω_0 is the eigenfrequency closest to the pump, D_1 is the microresonator FSR, and μ is the relative mode number from the pumped mode; high-order dispersion terms are neglected), κ is the pumped mode linewidth, $\zeta = 2(\omega_0 - \omega_{\mathrm{gen}})/\kappa$ is the normalized pump frequency detuning (with ω_{gen} being the laser generation frequency), and $f = \sqrt{P/P_{\mathrm{th}}}$ is the normalized pump amplitude equal to the ratio of pump power to the nonlinear threshold power,

$$P_{\mathrm{th}} = \frac{\omega_0 n_g^2 V_{\mathrm{eff}}}{8cn_2 Q^2 \eta}, \qquad (3)$$

where $Q = \omega_0/\kappa$ is the loaded quality factor, n_2 is the Kerr nonlinear refractive index, n_g is the microresonator mode group index, and V_{eff} is the microresonator effective mode volume. We should note that (1) is exact only for a nonlinear Schrödinger equation that is called the undumped, undriven Lugiato-Lefever equation, which is a limit case at $\zeta \gg 1$ [26]. This limitation is also in line with a natural demand for the soliton width to be smaller than the microresonator circumference, $\sqrt{d_2/\zeta} \ll 2\pi$. As we see further, this brings limitations to the theories based on this formalism. The output average power of solitons can be easily calculated by summing the mode components of the hyperbolic-secant-squared-shaped comb power [22] and recalculating the corresponding output. Using the transmittance coefficient from the ring resonator to the straight waveguide $T^2 = \eta \kappa t_{\mathrm{rt}}$, where $t_{\mathrm{rt}} = n_{\mathrm{eff}}L/c$ is the round-trip time [31], we obtain

$$P_{\mathrm{soliton}}^{\mathrm{out}} = \frac{8\eta^2}{\pi}\sqrt{d_2\zeta}\, P_{\mathrm{th}}, \qquad (4)$$

where $\eta = \kappa_c/\kappa$ is the normalized coupling rate or coupling efficiency ($\eta = 1/2$ for critical coupling) and κ_c is the coupling rate. Note that we consider anomalous GVD ($D_2 > 0$) and use the negative detuning definition, where the solitons exist at positive ζ. In this context, it is convenient to have a dimensional constant independent of the coupling efficiency. Therefore, we introduce the minimal threshold power $P_0 = \frac{27}{32}\frac{n_g^2 V_{\mathrm{eff}}\kappa_0^2}{cn_2\omega_0}$, where $\kappa_0 = \kappa - \kappa_c$ is the microresonator intrinsic decay rate. Then, the parametric instability threshold power is rewritten as follows:

$$P_{\mathrm{th}} = \frac{4P_0}{27}\frac{1}{\eta(1-\eta)^2}. \qquad (5)$$

The minimal threshold power P_0 is achieved at $\eta = 1/3$, which corresponds to the undercoupling regime, while the threshold power at critical coupling is 1.2 times higher. Remarkably, fulfilling the criterion $\eta = 1/3$ coincides with the optimal coupling efficiency for the self-injection locking at

weak backscattering [32]. Then, dividing (4) by the input power at the coupler P, we immediately get η_{p2s}.

Experimentally, the soliton parameters are difficult to measure in the time domain because of the ultrabroad bandwidth required for their detection, while the optical power spectrum is usually easier to measure and enough to determine the average power of the soliton thanks to Parseval's theorem. The spectral representation of the solitons results in a frequency comb with a uniform phase under a hyperbolic-secant envelope (1), while the constant background field results in an addition to the central line (or carrier) at the pumped frequency. Thus, it is not straightforward to separate the background from the solitons. So it is easier to omit the whole central peak, thus leading to the pump-to-comb sidebands or simply pump-to-comb efficiency [22]:

$$\eta_{\mathrm{p2c}} = \frac{4\eta^2}{f^2}\left(\frac{2}{\pi}\sqrt{d_2\zeta} - \frac{d_2}{2}\right) = \eta_{\mathrm{p2s}} - \frac{4\eta^2}{f^2}\frac{d_2}{2}. \qquad (6)$$

The first summand is effectively "pump-to-soliton" efficiency η_{p2s}, and the subtracted term is the central line power of the hyperbolic-secant envelope. It can also be more informative for those who are more interested in sideband power than in total comb power. The major difference between these two efficiencies is their behavior with the increase of the soliton number [22]. The pump-to-soliton efficiency naturally grows linearly as the soliton powers increase, while the second grows slower and saturates near the maximum soliton number $N_{\mathrm{max}}^{\mathrm{sol}} \approx \sqrt{1/d_2}$ set by the minimum distance at which solitons do not interact with each other [14]. Equation (6) shows that both efficiencies decrease with the square of the pump amplitude, suggesting it should be as low as possible.

III. ANALYTICAL CONSIDERATION

In what follows, we study the pump-to-comb efficiency as the most informative one. Consider the parameters constituting the definition (6). Generally, the detuning ζ is a free parameter. Obviously, it should be as large as possible for higher efficiency. However, stabilization of ζ is required to ensure the locking of the system to the desired regime despite the influence of various fluctuations [26]. The easiest way to achieve this stabilization is the self-injection-locking (SIL) mechanism [33], which locks the pump frequency to the microresonator eigenfrequency. As a result, we have two key ways to fix the range of the optimal detuning: (i) the maximum possible detuning enabling soliton generation (cutoff) $\zeta^{\mathrm{max}} = \pi^2 f^2/8$ and (ii) the detuning provided by the nonlinear SIL regime [22,34] $\zeta^0 = 2\sqrt{3}\sinh[\frac{1}{3}\operatorname{arcsinh}(\frac{3\sqrt{3}}{4}f^2)]$. We can see that $\zeta^0 \leqslant \zeta^{\mathrm{max}}$ for $f > 1.05$. For small pump powers, which are optimal for achieving high generation efficiency, both boundary limits converge to $\zeta \approx 1.38$, with ζ^{max} being hard (or impossible) to reach.

It is important to note that neither the SIL nor maximal detunings depend on the GVD coefficient. Thus, the pump-to-comb efficiency, (6), has a global maximum over the dispersion coefficient

$$\eta_{\mathrm{p2c}} = \frac{8\eta^2}{f^2}\frac{\zeta}{\pi^2}, \quad d_2 = \frac{4\zeta}{\pi^2}, \qquad (7)$$
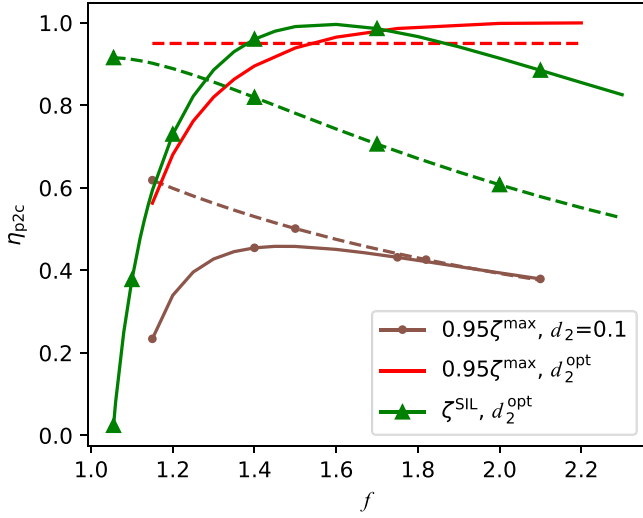
FIG. 1. Pump-to-comb conversion efficiency vs normalized pump amplitude for different values of effective pump frequency detuning and normalized dispersion coefficient. Solid lines show the numerical modeling, and dashed lines show the analytical expression (6). All quantities are plotted in dimensionless units.

FIG. 2. Pump-to-comb conversion efficiency vs coupling rate and internal losses calculated via (9) for fixed pump power. $\zeta = \zeta^{\max}$, and $D_2/\kappa_{\max} = 0.0143$. The dotted and dash-dotted lines correspond to the critical and minimal threshold couplings. The red solid curve shows $f = 2$ [the isocontour for this is $\bar{\kappa}_0 = (\bar{\kappa}_c^{1/3} - \bar{\kappa}_c)\kappa_{\max}/f$]. All quantities are plotted in dimensionless units.

while the pump-to-soliton efficiency η_{p2s} is monotonic over d_2. We can see that the global maximum of the pump-to-comb efficiency η_{p2c} is 100% at $\eta = 1$ regardless of the pump power (in the soliton-existence range) if we lock to the maximal detuning (see the dashed line in Fig. 1) and 90.9% for the SIL state at the near-threshold pump (see the dashed line with triangles in Fig. 1). Note that the comb width normalized to units of the intermode distance D_1 at the -3-dB level in this regime is $N_{\text{lines}} = \frac{2}{\pi}\sqrt{\frac{\zeta}{d_2}} \times 2 \operatorname{arccosh}\sqrt{2} \approx 1.76$. This number effectively shows a number of comb-line pairs around the pump above the -3-dB level. Here we come to the trade-off problem between the efficiency and the number of comb lines. The optimum described by (7) gives quite high dispersion values ($d_2 \geqslant 0.45$), revealing two challenges to be addressed. First, the experimental realization will require special resonator engineering [35–39]. Until now in most reported experiments values of $d_2 < 0.1$ were used as low dispersion allows for wider combs. Second, the validity of the analytical analysis as $d_2 \geqslant 1$ leads to $N_{\text{sol}}^{\max} < 1$, coinciding with the state when the width of the hyperbolic-secant-squared soliton becomes comparable to the microresonator circumference. Although the soliton still exists for greater dispersion values, lower pump, and detunings (for the SIL optimum), the hyperbolic secant ceases to be a proper stationary solution, and formula (4) becomes inaccurate. So we performed a numerical analysis of dissipative Kerr soliton properties using the Lugiato-Lefever-equation formalism [40,41]. This study showed that expression (6) is accurate only close to (but not exactly at) the cutoff detunings and $f > 2$ (see Fig. 1, solid lines). For SIL detuning, there is also a possibility of reaching 100% efficiency (see Fig. 1, lines with triangles), found numerically. More details are presented in Sec. IV. Note also that the desired high value of the second-order dispersion justifies the neglect of higher-order dispersion terms that have a strong
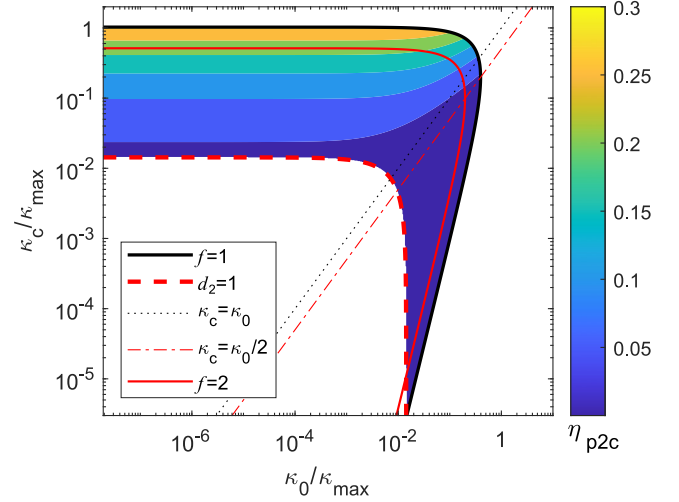
impact in the regime of vanishing group-velocity dispersion [20,42–46].

To get deeper insight into the problem, we continue studying Eq. (6) for the near-cutoff detuning, where the analytic solution is still accurate. We have several restrictions on the parameters. First, the normalized pump amplitude should be greater than 1 for soliton generation to be possible, and then f must be greater than 2 for the analytics to be valid. Second, the soliton should fit the ring, which can be controlled with $d_2 < 1$. This restriction also makes the number of lines $N_{\text{lines}} > 1$ (for $\zeta \approx 1$), which is quite close to the natural demand for having more than one line pair in the comb around the pump. Last, but not least, the coupling efficiency $\eta \in [0; 1)$ by definition. Outstandingly, these restrictions are independent of the pump frequency detuning and choice of conversion-efficiency definition.

A. Fixed pump power and dispersion

First, we consider the case of fixed pump power P and second-order dispersion D_2. Figure 2 shows the dependence of η_{p2c} on the coupling rate κ_c and internal losses κ_0 for the cutoff detuning with other fixed parameters (silicon nitride [22]). We can see that for fixed pump power κ_c and κ_0 cannot be chosen arbitrarily. Using (5) and $f = 1$, we introduce a maximal possible coupling rate for solitons to exist at a given pump power:

$$\kappa_{\max} = \sqrt{\frac{27P}{4P_0}}\kappa_0 = \sqrt{\frac{8cn_2\omega_0 P}{n_g^2 V_{\text{eff}}}}. \qquad (8)$$

For a desired normalized pump amplitude f at a given pump power the value which bounds the coupling κ_c is $\kappa_{\max}/f$ (see the horizontal part of the upper black curve in Fig. 2), and for the maximal internal loss, bounding κ_0 is $\sqrt{4/27}\kappa_{\max}/f$ (see the intersection of the upper black line and dash-dotted

line in Fig. 2). Note that $\kappa_{\max}$ does not actually depend on κ_0 as $P_0 \propto \kappa_0^2$ and thus consists only of other trivial parameters and pump power. To increase the level of generalization, we normalize all rate coefficients to the maximal coupling rate at given f and dispersion to the maximal coupling rate. Then for the pump-to-comb efficiency (6), we get

$$\eta_{\text{p2c}} = \frac{4\bar{\kappa}_c}{\bar{\kappa}_0 + \bar{\kappa}_c} [\sqrt{\bar{d}_2 \bar{\kappa}_c} - \bar{d}_2(\bar{\kappa}_0 + \bar{\kappa}_c)]. \quad (9)$$

Here $\bar{\kappa}_c = \kappa_c f/\kappa_{\max}$, $\bar{\kappa}_0 = \kappa_0 f/\kappa_{\max}$, and $\bar{d}_2 = D_2/2/\kappa_{\max}$. We also used $\zeta = \frac{\pi^2 f^2}{8}$ because we showed in the previous section that the theory works better near the cutoff.

Note again that at fixed pump power, we can operate with different normalized pump amplitudes f by choosing different coupling and loss rate combinations and get different efficiencies (see Fig. 2, solid red curve, $f = 2$, for example)]. An important observation is that the maximum efficiency always lies on the boundary $f = 1$ curve, confirming our previous speculations. A numerical study showed that the analytical solution is not accurate for low $f < 2$, after which the efficiency drops. So for both definitions of the efficiency and both maximum detuning values we can use $f = 2$ (e.g., the normalized pump should be minimized closer to the modulational instability threshold) and strong overcoupling $\eta = 1$ to maximize the conversion. The maximum value for (9), found in (κ_c, κ_0) substituted with $(\kappa_{\max}/f, 0)$ (that is, $\eta = 1$ and $d_2 = D_2/2/\kappa_{\max}$), can be written as $\eta_{\text{p2c}} \approx 4(\sqrt{\bar{d}_2/f} - \bar{d}_2/f)$. For a typical 1-THz Si$_3N_4$ microresonator [22], $P_0 \approx 9$ mW, and $\kappa_0 = 188$ MHz. Then for pump power $P \approx 40$ mW, the maximal coupling rate is $\kappa_{\max} \approx 1$ GHz. Having $D_2 \approx 14.3$ MHz and $f = 2$, we get $\eta_{\text{p2c}} = 22\%$ for a single-soliton comb.

B. Fixed normalized pump amplitude

Now we consider the case of fixed normalized pump f, and we optimize the dispersion and pump power or coupling. In the previous sections, we saw that the normalized pump amplitude governs the comb generation regime, strongly influencing the efficiency and analytic validity. After we fix f the detuning values $\zeta^{\max}$ and ζ^0 become fixed, and expression (6) has two free parameters: the normalized dispersion coefficient d_2 and coupling coefficient η. The latter is the easiest to tune. However, the first parameter also depends on the coupling, so it is better to extract it explicitly for further optimization. Considering (5), the optimal pumping regime over f imposes restrictions on the coupling:

$$\hat{\kappa}_c = \frac{\kappa_c}{\kappa_0} = 3\frac{f_0}{f} \sin\left(\frac{1}{3}\arccos\frac{f}{f_0} + \frac{\pi}{6}\right) - 1, \quad (10)$$

where we introduce the normalized pump amplitude to the minimal threshold $f_0 = \sqrt{P/P_0}$ for simplicity. Formula (10) directly connects the required pump power with the optimal coupling level without using other parameters. This dependence is shown in Fig. 3. For large pump $f_0/f \gg 3$ it tends to $\hat{\kappa}_c = 3\frac{\sqrt{3}}{2}\frac{f_0}{f} - \frac{3}{2}$. Note that the minimal possible pump power $P = P_0 f_x^2$ to maintain a desired f is obtained at subcritical coupling $\kappa_c = \kappa_0/2$, which is in agreement with (5). Note also that in this case it is more convenient to use rates normalized to the internal loss as $\kappa_{\max}$ is not fixed. Similarly, the minimal
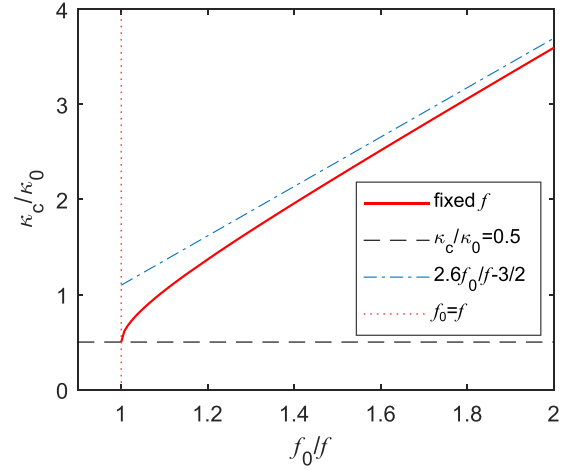

FIG. 3. Coupling efficiency needed to maintain fixed f for the given pump power calculated from (10) (solid line). The dash-dotted line shows its asymptote for high pump power. All quantities are plotted in dimensionless units.

threshold power P_0 was not used in the previous section, being fixed only now.

Combining expressions (10) and (6), we obtain the formula for the dependence of the pump-to-comb efficiency on the pump amplitude normalized to the minimal threshold f_0, normalized coupling rate $\hat{\kappa}_c$, and target pump amplitude f:

$$\eta_{\text{p2c}} = \frac{8\hat{\kappa}_c f^2}{27 f_0^2} \left[f\sqrt{6\hat{d}_2\left(\frac{f_0^2 \hat{\kappa}_c}{4f^2}\right)^{1/3}} - \hat{d}_2 \right]. \quad (11)$$

Here $\hat{\kappa}_c = \kappa_c/\kappa_0$, $\hat{d}_2 = D_2/\kappa_0$, and we also used $\zeta = \frac{\pi^2 f^2}{8}$. As we fix the detuning and combine (10) and (11), this dependence can be plotted as a color map with only two free parameters: $\hat{d}_2 = D_2/\kappa_0$ and $\hat{\kappa}_c = \kappa_c/\kappa_0$ (see Fig. 4). We can see that for a fixed dispersion value there is an optimum over the coupling value (light green solid line in Fig. 4). It can be shown that for small GVD, it tends to $\kappa_c/\kappa_0 \approx 4$. In the left panel of Fig. 4 we use $f = 1$ as the most illustrative case, although that is not quite correct. For greater f the global maximum will shift up and eventually go above the $d_2 = 1$ line. The right panel of Fig. 4 shows the efficiency map for $f = 2$. Comparing it with the left panel, we can see that the maximum goes beyond $d_2 = 1$ with growing f. The other important observation is that the number of lines grows with f.

Another essential way to represent the efficiency map is to recalculate d_2 as the number of comb lines above the -3-dB level for given f_0. So we present a map of the pump-to-comb efficiency in coordinates f_0-N_{lines} in Fig. 5. We can see that the pump-to-comb efficiency is reduced as the number of lines increases and its growth saturates as the power increases.

For some essential applications, the absolute power of the generated comb is a more critical parameter than the efficiency. Formula (4) suggests that it does not directly depend on the pump power and increases mainly with the threshold power. The increased pump power (for fixed threshold) provides greater possible detuning values; however, this effect is weaker.
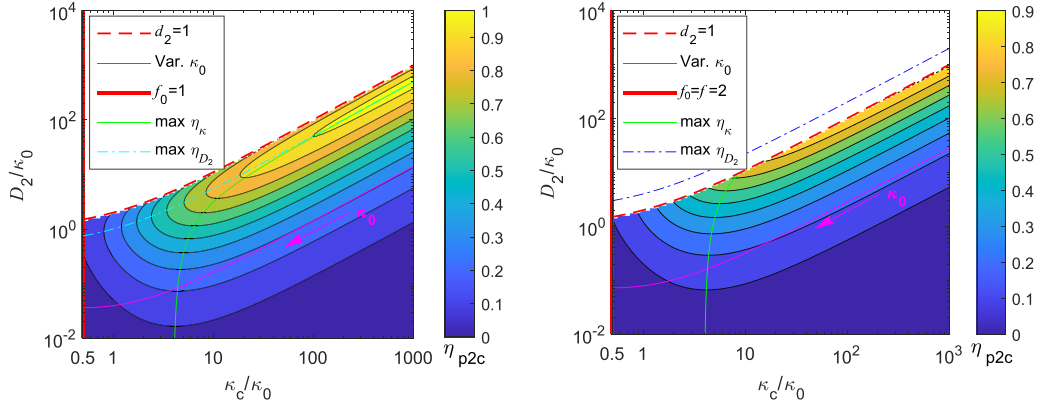
FIG. 4. Pump-to-comb conversion efficiency vs intrinsic-loss-normalized coupling κ_c/κ_0 and dispersion D_2/κ_0 via (6) and (10) for $\zeta = \zeta^{\max}$ and fixed f. The left panel shows $f = 1$, and the right panel shows $f = 2$. The thick vertical line is the minimal $P/P_0 = 1$, the dark red dashed line is $d_2 = 1$, and the thin pink solid curve is the tuning of the intrinsic loss for $D_2/\kappa_{\max} = 0.0143$. The light green solid line is the optimal coupling for fixed D_2/κ_0, and the dash-dotted curve is the optimum (7). All quantities are plotted in dimensionless units.

In Fig. 6, the total comb power without the pumped mode normalized to P_0 ($P_{\text{out}} = \eta_{\text{p2c}}P$) is shown depending on the normalized pump power f_0^2 for different coupling rates. Red lines 2 corresponds to the threshold pumping case with $f = 1$, so the coupling changes with the pump power, according to (10) (the solid line shows the maximum detuning, and the dashed line shows locked detuning). We can see that this regime is always superior to the case of fixed coupling (see lines 3, 4, and 5). The lines in Fig. 6 do not change if the minimal threshold power P_0 is changed by means of the material parameters. If P_0 is increased by means of the microresonator intrinsic loss κ_0, then the optimal curve goes up (see blue lines 1 and compare with red lines 2 in Fig. 6). This means that although we should increase both the pump and the threshold power for higher output comb power, the microresonator intrinsic losses should never be increased.

It is also useful to add the line corresponding to a variation of the intrinsic losses to the previous efficiency maps in the right panels of Figs. 4 and 5. We should note that both N_{lines} and P/P_0 depend on the microresonator intrinsic loss rate κ_0, and if we tune it while keeping other parameters fixed, the working point will follow the curve $\hat{d}_2 = f_0 D_2/\kappa_{\max}$, where $f_0 \propto 1/\kappa_0$. This can also be written in terms of the comb width

(in units of D_1):

$$N_{\text{lines}}(f_0) = \frac{4 \operatorname{arccosh}\sqrt{2}}{\pi} \sqrt{\frac{\zeta}{D_2}\sqrt{\frac{27P\kappa_0^2}{4P_0}}\left(1 - \frac{1}{27f_0}\right)}. \quad (12)$$

This path is shown in Figs. 4 and 5 for $D_2/2\pi = 14.3$ MHz and $\kappa_{\max}/2\pi = 1$ GHz by a thin pink solid curve, and an arrow shows the way of κ_0 increase. This line also represents the same configurations as the upper branch of the black line in Fig. 2. This analysis also shows that the high intrinsic losses are not optimal for the conversion efficiency.

To conclude this section we have to note that although such analytical derivations may be inaccurate in regions of small pump and detuning, they lead to general relations and deeper insight into the conversion-efficiency problem. Enhancements of the theory can be done in terms of including higher dispersion orders and soliton form corrections, but this can make it less transparent or analytically irresolvable, and thus such complications are not fully justified. Thus, having the regions of interest highlighted by simple approximations, we feel it is reasonable to proceed directly to numerical study.
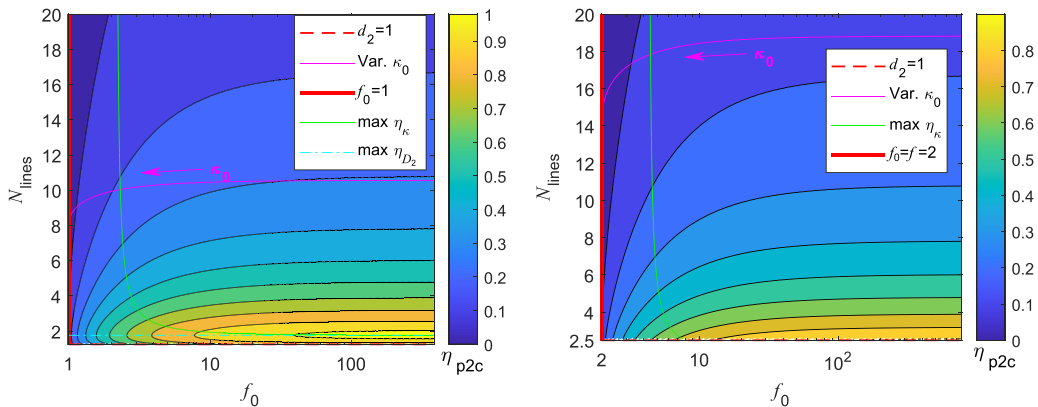

FIG. 5. Pump-to comb-efficiency vs f_0 and the number of comb lines calculated via (6) and (10). Additional lines and parameters are the same as in the right panel of Fig. 4. All quantities are plotted in dimensionless units.
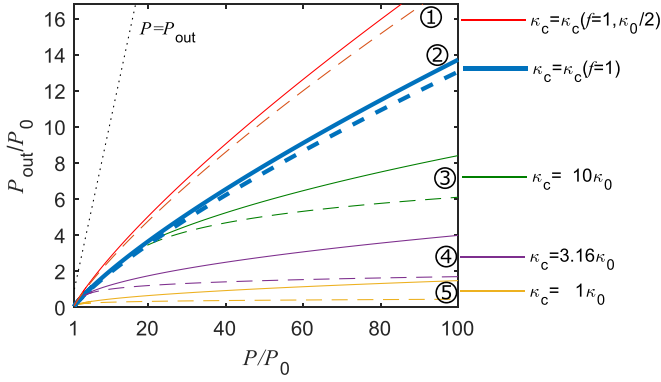
FIG. 6. Total comb power without the pumped mode, normalized to P_0, vs the normalized pump power for different coupling rates. Solid lines correspond to maximum detuning, and dashed lines correspond to locked detuning. Lines 1 and 2 correspond to the threshold pumping case $f = 1$ according to (10). Lines 3, 4, and 5 correspond to different fixed couplings. Blue lines 1 correspond to the case with $f = 1$ and 2 times less internal losses. The black dotted line shows $P = P_{out}$, e.g., the 100% efficiency limit. System parameters are $\kappa_0/2\pi = 188$ MHz and $D_2/2\pi = 14.3$ MHz. All quantities are plotted in dimensionless units.

IV. NUMERICAL MODELING

As noted in the previous sections, the analytical approximation (1) may be inaccurate for small detunings ζ and low pump amplitude f. Here we perform the numerical modeling using the pulse propagation in the Lugiato-Lefever equation formalism [40,41] and compare the results with the analytical solution. We also numerically calculate the efficiency to make a comparison with (6) for different combinations of parameters, including the optimum (7) for cutoff and SIL detunings. In this study we find that the solution (1) actually diverges from the numerically obtained wave forms near cutoff detuning at low pump power.

For numerical analysis, we solve the Lugiato-Lefever equation

$$\frac{\partial a}{\partial \tau} = i \frac{d_2}{2} \frac{\partial^2 a}{\partial \varphi^2} - [1 + i\zeta]a + i|a|^2 a + f \quad (13)$$

with the hyperbolic-secant initial condition and propagate until the solution reaches the stationary regime. Here a is the intracavity field distribution over the azimuthal angle φ (the Fourier transform of the modal fields a_μ), and time is normalized to the total decay rate $\tau = \kappa t / 2$. Figure 7 shows the simulated and analytical soliton profiles for the cutoff and SIL detunings with the corresponding optimal dispersion (7). We can see that approaching $f = 1$, the form of the soliton does not change as significantly as the theory predicts. This suggests that the analytical soliton profile has the wrong phase dependence for low f. For low detuning values satisfactory correspondence is not found.

Then we take the Fourier transform of a and sum up all the modal powers excluding the central one. Assuming overcoupling ($\eta = 1$), we are left with only three free parameters, the detuning ζ, the dispersion d_2, and the pump amplitude f, so we can build a cloud of efficiency values to compare with (6).

In Fig. 8 the simulated efficiency values (left) and their difference from the analytical values (6) (right) are shown. The optimal parameter combinations (7) for cutoff and SIL detunings are shown with blue and orange lines. We can see that as the pump amplitude reduces to 1, the analytic solution starts to overestimate the numerical one (see also the left panel of Fig. 9). At the same time, the values at small detunings (e.g., in the self-injection-locking regime) are underestimated (see also the right panel of Fig. 9). For $f < 1.5$ the efficiency is always less than 90%. The maximal value of 100% appears at $f = 1.6$ at the SIL detuning (and optimal $d_2 \approx 1$) and then travels to the cutoff, reaching it near $f = 2$ (and optimal $d_2 = 2$), where the analytical hyperbolic-secant-squared solution becomes precise. Generally, in the region of bad analytical approximation, $f < 2$, the optimal detunings will be slightly lower than analytically predicted, and dispersion will be slightly higher. The highest concentration of the high-efficiency regime points is near $f \approx 1.6$. The right panel of Fig. 9 also shows that the soliton-existence region over detuning is different for different pump amplitudes. Note that while the cutoff detuning is strict for soliton existence,
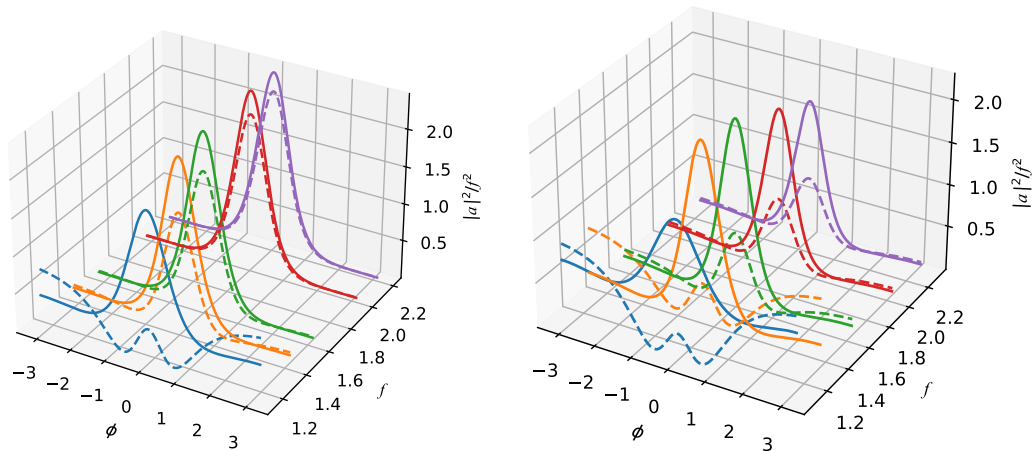

FIG. 7. Simulated soliton profiles (solid lines) and their analytical approximations (dashed lines) for the different values of the normalized pump amplitude f. The left panel shows the results for the near-cutoff ($\approx 0.95 \zeta_{eff}^{max}$) detunings and optimal dispersion coefficient (7). The right panel shows the results for the SIL detuning and optimal dispersion coefficient (7). All quantities are plotted in dimensionless units.
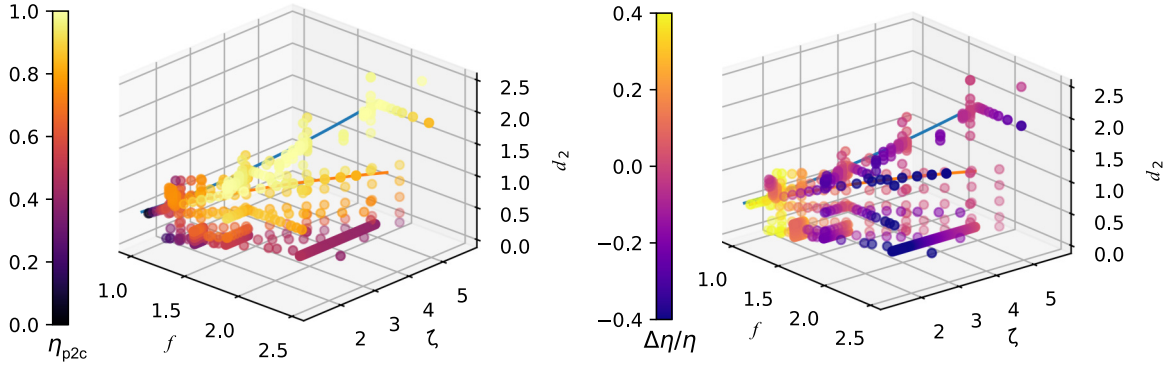
FIG. 8. Simulated pump-to-comb conversion efficiency (left) and its difference from the analytical approximation (6) (right). The blue and orange lines correspond to the optimal dispersion value (7) for the near-cutoff detuning and for the locked detuning. All quantities are plotted in dimensionless units.

the SIL detuning is generally higher than the lower existence boundary.

In the literature one may find the next order approximation for the soliton form [47,48]. We should note, however, that although it gives better results for lower detunings, this modification still does not work for low normalized pump amplitudes, which are of the most interest, while at high detunings the simple approximation is precise.

V. BACKWARD WAVE

The reader should note that although the SIL detunings have been considered, no simulation including the locking mechanism has actually been performed; that is, no laser and pump frequency dynamics have been considered in (13). Until now we have also restricted ourselves to only the forward wave. It was shown, however, that the existence of a backward wave influences soliton generation and should be taken into consideration [49–52]. This influence increases with increas-

ing backscattering and also with decreasing pump power [51]. Obviously, backscattering will reduce the efficiency, letting the power into the backward wave. Additional analysis was performed using the bidirectional approach [51,53,54],

$$\frac{\partial a}{\partial \tau} = i\frac{d_2}{2}\frac{\partial^2 a}{\partial \varphi^2} - (1+i\zeta)a + i(|a|^2 + 2U_b)a + i\beta b(-\varphi) + f,$$

$$\frac{\partial b}{\partial \tau} = i\frac{d_2}{2}\frac{\partial^2 b}{\partial \varphi^2} - (1+i\zeta)b + i(|b|^2 + 2U_a)b + i\beta a(-\varphi)$$

for several key points of the parameter space. Here b stands for the backward-wave amplitude, β is the normalized backscattering coefficient [equal to the ratio of the linear mode-splitting value and loaded microresonator linewidth], and $U_a = \int |a(\varphi)|^2 \frac{d\varphi}{2\pi}$ and $U_b = \int |b(\varphi)|^2 \frac{d\varphi}{2\pi}$ are the average intracavity powers of the waves. It was revealed that for the most interesting values of the pump power ($f > 1.4$) the backscattering of $\beta < 0.1$ does not significantly harm the efficiency. Again, we see that for higher backscattering soliton
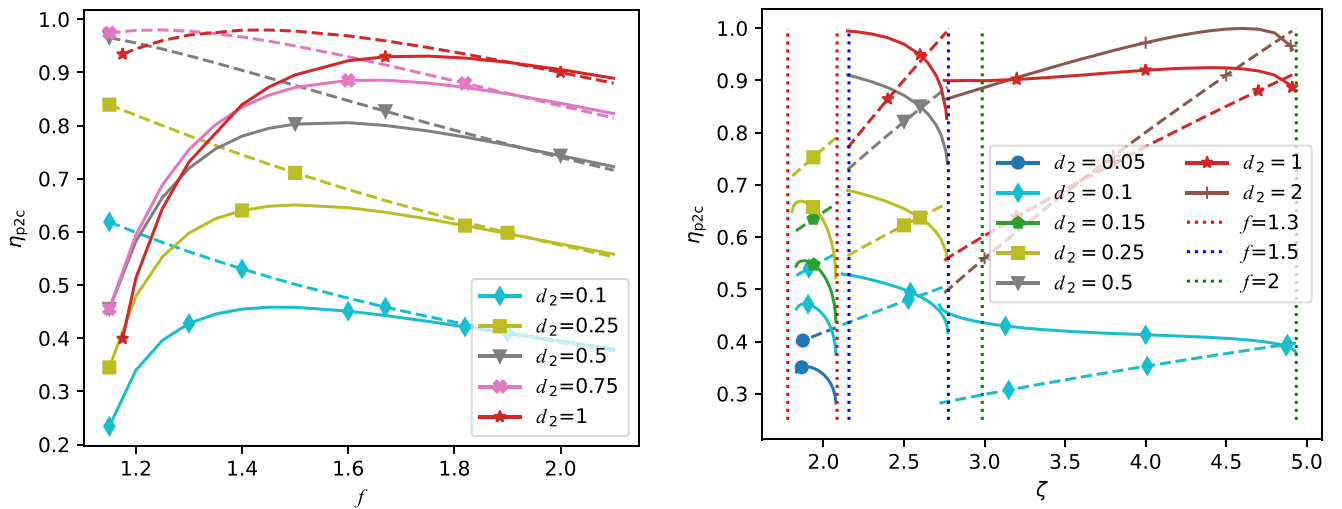

FIG. 9. Simulated pump-to-comb conversion efficiency (solid lines) and the analytical approximation (6) (dashed lines) for fixed dispersion. The left panel shows the pump sweep for near-cutoff ($\approx 0.98\zeta_{\mathrm{eff}}^{\max}$) detunings and different dispersion coefficients d_2. The right panel shows the detuning sweep for different normalized pump amplitudes f (lines inside corresponding detuning boundaries) and different dispersion coefficients d_2 (line colors); the dotted vertical lines show the SIL (left) and cutoff (right) detunings for the corresponding pump amplitude. Note that while the cutoff detuning is strict for soliton existence, the SIL detuning is generally higher than the lower existence boundary. All quantities are plotted in dimensionless units.
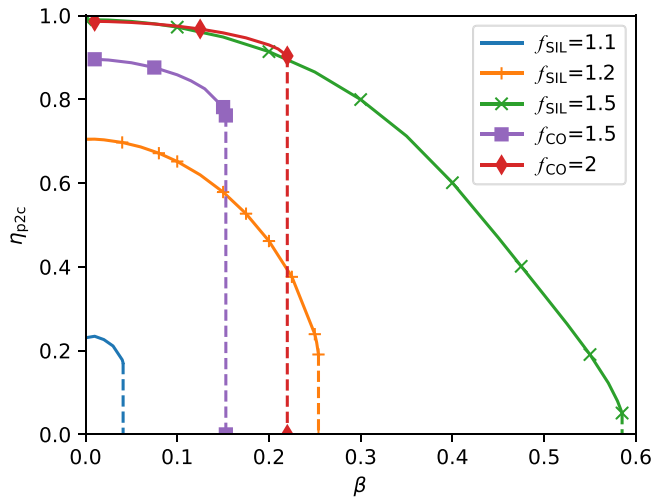
FIG. 10. Pump-to-comb dependence on the normalized backscattering coefficient β. SIL and CO stand for SIL detuning and cutoff detuning. Dispersion is chosen to be optimal (7). Vertical dashed lines show the backscattering-related cutoff. All quantities are plotted in dimensionless units.

generation is hindered (see vertical dashed lines in Fig. 10). We should note that values of $\beta \gg 1$ can be controlled effectively in specially designed photonic crystal ring resonators [55]. It was stated in [55] that possible large values of $\beta \gg 1$ allow for a greater change in the effective detuning inside the locked state, which can partially compensate for the loss of efficiency due to the backward wave.

VI. CONCLUSION

In conclusion, an analytical guideline was proposed to optimize the soliton microcomb generation efficiency in a high-Q optical microresonator. The developed theory analyzed the combination of pump amplitude and detuning, microresonator second-order dispersion, and laser-to-microresonator coupling rate and showed a theoretical solution for reaching

100% in a simple single-resonator scheme. The analytical calculation can predict the optimal parameters for pumps above $f = 2$. For a lower pump, optimal detunings will be slightly lower, and dispersion will be slightly higher due to approximation failure, and direct numerical calculation is encouraged. Generally, the system should be pumped not far from the generation threshold ($f \approx 1.6$). This regime has a smaller optimal dispersion value and maximal efficiency for most detuning values and ensures no wasted pump power; more pump power does not change the soliton amplitude and average power. For this purpose, the coupling should be increased, or the pump power should be reduced. In practical terms, a trade-off between the efficiency and number of comb lines should be chosen at the design stage, forcing the appropriate dispersion profile to be tailored (by means of material and geometry engineering) for an achievable coupling. However, it should be noted that dispersion engineering can also affect the threshold power and coupling due to the changes in the effective mode volume and effective index. Additionally, the regime of self-injection locking of the pump laser can help to maintain the necessary pump frequency detuning since, at threshold pumping, the soliton-existence range in the spectral domain is quite narrow. Although the analytical theory was found to fail in the low-pump, low-detuning region, numerical simulations showed the optimum point is near $f \approx 1.6$, $d_2 \approx 0.95$. Finally, to increase the absolute comb power, the same strategy should be applied, with the only difference being that the generation threshold power should be maximized. To this aim, the safest approach is to increase the coupling efficiency significantly while keeping the intrinsic losses low.

[1] T. J. Kippenberg, R. Holzwarth, and S. A. Diddams, Science **332**, 555 (2011).

[2] Y. K. Chembo, Nanophotonics **5**, 214 (2016).

[3] A. Pasquazi, M. Peccianti, L. Razzari, D. J. Moss, S. Coen, M. Erkintalo, Y. K. Chembo, T. Hansson, S. Wabnitz, P. Del'Haye, X. Xue, A. M. Weiner, and R. Morandotti, Phys. Rep. **729**, 1 (2018).

[4] A. L. Gaeta, M. Lipson, and T. J. Kippenberg, Nat. Photonics **13**, 158 (2019).

[5] A. Kovach, D. Chen, J. He, H. Choi, A. H. Dogan, M. Ghasemkhani, H. Taheri, and A. M. Armani, Adv. Opt. Photon. **12**, 135 (2020).

[6] M. Nie, Y. Xie, B. Li, and S.-W. Huang, Prog. Quantum Electron. **86**, 100437 (2022).

[7] M.-G. Suh, Q.-F. Yang, K. Y. Yang, X. Yi, and K. J. Vahala, Science **354**, 600 (2016).

[8] M. Kues, C. Reimer, J. M. Lukens, W. J. Munro, A. M. Weiner, D. J. Moss, and R. Morandotti, Nat. Photonics **13**, 170 (2019).

[9] J. Riemensberger, A. Lukashchuk, M. Karpov, W. Weng, E. Lucas, J. Liu, and T. J. Kippenberg, Nature (London) **581**, 164 (2020).

[10] P. Marin-Palomo, J. N. Kemal, M. Karpov, A. Kordts, J. Pfeifle, M. H. P. Pfeiffer, P. Trocha, S. Wolf, V. Brasch, M. H. Anderson, R. Rosenberger, K. Vijayan, W. Freude, T. J. Kippenberg, and C. Koos, Nature (London) **546**, 274 (2017).

[11] M.-G. Suh, X. Yi, Y.-H. Lai, S. Leifer, I. S. Grudinin, G. Vasisht, E. C. Martin, M. P. Fitzgerald, G. Doppmann, J. Wang, D. Mawet, S. B. Papp, S. A. Diddams, C. Beichman, and K. Vahala, Nat. Photonics **13**, 25 (2019).

[12] T. J. Kippenberg, A. L. Gaeta, M. Lipson, and M. L. Gorodetsky, Science **361**, eaan8083 (2018).

[13] Y. Sun, J. Wu, M. Tan, X. Xu, Y. Li, R. Morandotti, A. Mitchell, and D. J. Moss, Adv. Opt. Photonics **15**, 86 (2023).

[14] M. Karpov, M. H. P. Pfeiffer, H. Guo, W. Weng, J. Liu, and T. J. Kippenberg, Nat. Phys. **15**, 1071 (2019).

[15] X. Xue, X. Zheng, and B. Zhou, Nat. Photonics **13**, 616 (2019).

[16] J. M. C. Boggio, D. Bodenmüller, S. Ahmed, S. Wabnitz, D. Modotto, and T. Hansson, Nat. Commun. **13**, 1292 (2022).

[17] X. Xue, P.-H. Wang, Y. Xuan, M. Qi, and A. M. Weiner, Laser Photonics Rev. **11**, 1600276 (2017).

[18] N. M. Kondratiev, V. E. Lobanov, E. A. Lonshakov, N. Y. Dmitriev, A. S. Voloshin, and I. A. Bilenko, Opt. Express **28**, 38892 (2020).

[19] B. Y. Kim, Y. Okawachi, J. K. Jang, M. Yu, X. Ji, Y. Zhao, C. Joshi, M. Lipson, and A. L. Gaeta, Opt. Lett. **44**, 4475 (2019).

[20] Q.-X. Ji, W. Jin, L. Wu, Y. Yu, Z. Yuan, W. Zhang, M. Gao, B. Li, H. Wang, C. Xiang, J. Guo, A. Feshali, M. Paniccia, V. S. Ilchenko, A. B. Matsko, J. E. Bowers, and K. J. Vahala, Optica **10**, 279 (2023).

[21] J. Li, C. Bao, Q.-X. Ji, H. Wang, L. Wu, S. Leifer, C. Beichman, and K. Vahala, Optica **9**, 231 (2022).

[22] N. Y. Dmitriev, S. N. Koptyaev, A. S. Voloshin, N. M. Kondratiev, K. N. Min'kov, V. E. Lobanov, M. V. Ryabko, S. V. Polonsky, and I. A. Bilenko, Phys. Rev. Appl. **18**, 034068 (2022).

[23] J. K. Jang, Y. Okawachi, Y. Zhao, X. Ji, C. Joshi, M. Lipson, and A. L. Gaeta, Opt. Lett. **46**, 3657 (2021).

[24] C. Bao, L. Zhang, A. Matsko, Y. Yan, Z. Zhao, G. Xie, A. M. Agarwal, L. C. Kimerling, J. Michel, L. Maleki, and A. E. Willner, Opt. Lett. **39**, 6126 (2014).

[25] J. Gärtner, P. Trocha, R. Mandel, C. Koos, T. Jahnke, and W. Reichel, Phys. Rev. A **100**, 033819 (2019).

[26] T. Herr, V. Brasch, J. D. Jost, C. Y. Wang, N. M. Kondratiev, M. L. Gorodetsky, and T. J. Kippenberg, Nat. Photonics **8**, 145 (2014).

[27] N. G. Pavlov, S. Koptyaev, G. V. Lihachev, A. S. Voloshin, A. S. Gorodnitskiy, M. V. Ryabko, S. V. Polonsky, and M. L. Gorodetsky, Nat. Photonics **12**, 694 (2018).

[28] A. S. Raja, A. S. Voloshin, H. Guo, S. E. Agafonova, J. Liu, A. S. Gorodnitskiy, M. Karpov, N. G. Pavlov, E. Lucas, R. R. Galiev, A. E. Shitikov, J. D. Jost, M. L. Gorodetsky, and T. J. Kippenberg, Nat. Commun. **10**, 680 (2019).

[29] B. Shen, L. Chang, J. Liu, H. Wang, Q.-F. Yang, C. Xiang, R. N. Wang, J. He, T. Liu, W. Xie, J. Guo, D. Kinghorn, L. Wu, Q.-X. Ji, T. J. Kippenberg, K. Vahala, and J. E. Bowers, Nature (London) **582**, 365 (2020).

[30] X. Yi, Q.-F. Yang, K. Y. Yang, and K. Vahala, Opt. Lett. **41**, 3419 (2016).

[31] M. L. Gorodetsky and V. S. Ilchenko, J. Opt. Soc. Am. B **16**, 147 (1999).

[32] R. R. Galiev, N. M. Kondratiev, V. E. Lobanov, A. B. Matsko, and I. A. Bilenko, Phys. Rev. Appl. **14**, 014036 (2020).

[33] N. M. Kondratiev, V. E. Lobanov, A. V. Cherenkov, A. S. Voloshin, N. G. Pavlov, S. Koptyaev, and M. L. Gorodetsky, Opt. Express **25**, 28167 (2017).

[34] N. M. Kondratiev, V. E. Lobanov, A. E. Shitikov, R. R. Galiev, D. A. Chermoshentsev, N. Y. Dmitriev, A. N. Danilin, E. A. Lonshakov, K. N. Min'kov, D. M. Sokol, S. J. Cordette, Y.-H. Luo, W. Liang, J. Liu, and I. A. Bilenko, Front. Phys. **18**, 21305 (2023).

[35] I. S. Grudinin and N. Yu, Optica **2**, 221 (2015).

[36] S. Fujii and T. Tanabe, Nanophotonics **9**, 1087 (2020).

[37] S.-P. Wang, T.-H. Lee, Y.-Y. Chen, and P.-H. Wang, Micromachines **13**, 454 (2022).

[38] E. Lucas, S.-P. Yu, T. C. Briles, D. R. Carlson, and S. B. Papp, arXiv:2209.10294

[39] C. Zhang, G. Kang, J. Wang, Y. Pan, and J. Qu, Opt. Express **30**, 44395 (2022).

[40] Y. K. Chembo and C. R. Menyuk, Phys. Rev. A **87**, 053852 (2013).

[41] C. Godey, I. V. Balakireva, A. Coillet, and Y. K. Chembo, Phys. Rev. A **89**, 063814 (2014).

[42] C. Bao, H. Taheri, L. Zhang, A. Matsko, Y. Yan, P. Liao, L. Maleki, and A. E. Willner, J. Opt. Soc. Am. B **34**, 715 (2017).

[43] J. H. T. Mbé and Y. K. Chembo, J. Opt. Soc. Am. B **37**, A69 (2020).

[44] M. H. Anderson, W. Weng, G. Lihachev, A. Tikan, J. Liu, and T. J. Kippenberg, Nat. Commun. **13**, 4764 (2022).

[45] Z. Xiao, T. Li, M. Cai, H. Zhang, Y. Huang, C. Li, B. Yao, K. Wu, and J. Chen, Light: Sci. Appl. **12**, 33 (2023).

[46] S. Zhang, T. Bi, and P. Del'Haye, Laser Photonics Rev., 2300075 (2023).

[47] H. Guo, M. Karpov, E. Lucas, A. Kordts, M. H. P. Pfeiffer, V. Brasch, G. Lihachev, V. E. Lobanov, M. L. Gorodetsky, and T. J. Kippenberg, Nat. Phys. **13**, 94 (2017).

[48] X. Li, B. Shen, H. Wang, K. Y. Yang, X. Yi, Q.-F. Yang, Z. Zhou, and K. Vahala, Opt. Lett. **43**, 2567 (2018).

[49] S. Fujii, A. Hori, T. Kato, R. Suzuki, Y. Okabe, W. Yoshiki, A.-C. Jinnai, and T. Tanabe, Opt. Express **25**, 28969 (2017).

[50] Q.-F. Yang, X. Yi, K. Y. Yang, and K. Vahala, Nat. Photonics **11**, 560 (2017).

[51] V. E. Lobanov, A. E. Shitikov, R. R. Galiev, K. N. Min'kov, and N. M. Kondratiev, Opt. Express **28**, 36544 (2020).

[52] Z. Fan and D. V. Skryabin, Opt. Lett. **45**, 6446 (2020).

[53] N. M. Kondratiev and V. E. Lobanov, Phys. Rev. A **101**, 013816 (2020).

[54] D. V. Skryabin, OSA Continuum **3**, 1364 (2020).

[55] A. E. Ulanov, T. Wildi, N. G. Pavlov, J. D. Jost, M. Karpov, and T. Herr, arXiv:2301.13132.